Dyes and Pigments 163 (2019) 213–220

Contents lists available at ScienceDirect

Dyes and Pigments

journal homepage: www.elsevier.com/locate/dyepig

Universal materials for high performance violet-blue OLEDs ($CIE_y < 0.06$) and PhOLEDs

Zhong-Yi Wang[a], Jue-Wen Zhao[b], Bin Liu[c], Chen Cao[a], Peng Li[a], Qing-Xiao Tong[a,*], Si-Lu Tao[b,**]

[a] Department of Chemistry and Key Laboratory for Preparation and Application of Ordered Structural Material of Guangdong Province, Shantou University, Guangdong, 515063, PR China

[b] School of Optoelectronic Information, University of Electronic Science and Technology of China (UESTC), Chengdu, 610054, PR China

[c] Department of Physics, Fudan University, Shanghai, 200433, PR China

ARTICLE INFO

Keywords:
Universal materials
Deep-blue
Phenanthroimidazole
Organic light-emitting diodes
Twisted intramolecular charge-transfer

ABSTRACT

Deep blue emitters with good stability, high quantum yield, high triplet energy, and good carrier transporting properties are crucial for full color display and white solid lighting. To solve this, We designed, synthesized and characterized two bipolar deep-blue emitters 2-(4-(9,9′-spirobi[fluoren]-2-yl)phenyl)-1-phenyl-1H-phenanthro[9,10-d]imidazole (**2-PPI—SBF**) and 2-(4-(9,9′-spirobi[fluoren]-4-yl)phenyl)-1-phenyl-1H-phenanthro[9,10-d]imidazole (**4-PPI—SBF**). Both the materials show good stability, high quantum yield and high triplet energy. Equipped with their bipolar properties, 2-PPI—SBF and 4-PPI—SBF based non-doped devices show impressive performance with maximum external quantum efficiency (EQE) of 4.78% and 5.29% along with desirable color purity of CIE color coordinates of (0.154, 0.105) and (0.155, 0.058) respectively. Interestingly, the high triplet energy allows them to be used as a host for PhOLEDs. High performance green PhOLEDs based on 4-PPI—SBF show the maximum EQE, CE and PE of 16.79%, 64.09 cd/A and 67.92 l m/W respectively. And, high performance red PhOLEDs based on 2-PPI—SBF and 4-PPI—SBF were also achieved with the maximum EQE of 13.07% and 14.83%, respectively. Furthermore, 4-PPI—SBF-based WOLED shows high efficiencies with EQE_{max} of 12.27%, CE_{max} of 27.78 cd/A and PE_{max} of 32.68 l m/W. An efficient white OLED with CIE coordinates of (0.367, 0.305) which is slightly deviated from the values of the theoretical white point (0.33, 0.33) was obtained.

1. Introduction

During the past decade, organic light-emitting diodes (OLEDs) have been becoming indispensable both in commercial flat-panel displays and general lighting applications. Fluorescent materials have been widely used in commercial devices because of their high color purity and long operational lifetime. However, the internal quantum efficiency of traditional fluorescent is limited to 25%, as the recombination of injected electrons and holes generates the lowest excited triplet (T1) and singlet(S1) states at a ratio of 3:1 [1]. Compared with traditional fluorescent OLED, phosphorescent organic light-emitting diodes (PhOLEDs) can harvest both singlet and triplet excitons to achieve 100% internal quantum efficiency [2]. Nevertheless, high concentration of these emitters can easily lead to concentration quenching and triplet-triplet annihilation [3]. To overcome this demerit, they are typically dispersed in appropriate host materials with sufficiently high triplet energy in PhOLEDs. In addition,a host aims for OLED application is to reduce the production cost of materials, simplify the manufacturing process, and achieve high-performance full-color electroluminescence based on simple materials system and device structure. Currently, the tailor-made bipolar host materials consisting of both the electron-donating and electron-accepting units have aroused great attention in the area of phosphorescent OLEDs because they can provide more balanced carrier fluxes and simplify the device structure [4]. In addition, bipolar host materials can improve device performance and reduce efficiency roll-off compared to the traditional unipolar hosts [5]. Among them, a lot of phosphorescent hosts doped with $IrMDQ(acac)_2$ and $Ir(ppy)_3$ to show the high-efficiency red and green phosphorescent emission have been reported. However, non-doped devices based on those host materials exhibit poor color purity. Therefore, it is requisite to develop novel universal materials can not only achieve non-doped high-efficiency emission, but also act as a host material to sensitize lower-energy dopants for creating other colors and white emission.

A practical strategy has been applied to achieve high-performance

* Corresponding author.
** Corresponding author.
E-mail addresses: qxtong@stu.edu.cn (Q.-X. Tong), silutao@uestc.edu.cn (S.-L. Tao).

https://doi.org/10.1016/j.dyepig.2018.11.058
Received 1 October 2018; Received in revised form 29 November 2018; Accepted 29 November 2018
Available online 02 December 2018
0143-7208/

full color OLEDs by introducing the bipolar deep-blue emitting materials. But, as for the blue fluorophore, conjugation resulted from the intramolecular donor-acceptor interaction will lower the triplet energy. In order to overcome this drawback, many molecules with bipolar units were reported. Such as, phenanthroimidazole derivatives [6], and benzimidazole derivatives [7], and so on. In this paper, we reported two novel universal materials named 2-(4-(9,9′-spirobi[fluoren]-2-yl) phenyl)-1-phenyl-1H-phenanthro[9,10-d]imidazole (**2-PPI—SBF**) and 2-(4-(9,9′-spirobi[fluoren]-4-yl)phenyl)-1-phenyl-1H-phenanthro[9,10-d]imidazole (**4-PPI—SBF**). Phenanthroimidazole was used as bipolar unit, due to their high fluorescent quantum yields, relatively high triplet energy levels and good thermal stability [8]. Additionally, we introduced spirobifluorene (SBF) at C2 position of phenanthroimidazole, which possess a wide energy gap and a high triplet energy (E_T). They can be used as both non-doped deep blue emitters and bipolar host materials for deep-blue OLEDs, PhOLEDs and WOLED. Based-2-PPI—SBF and 4-PPI—SBF non-doped devices, the maximum EQE achieved 4.78% and 5.29% with desirable color purity of CIE (0.154, 0.105) and (0.155, 0.058). Interestingly, 4-PPI—SBF and 2-PPI—SBF are suitable to host various phosphors, including Ir(MDQ)$_2$(acac) (red), Ir(ppy)$_3$(acac) (green), with excellent performances. In addition, 4-PPI—SBF-based WOLED exhibits excellent device performance, the max EQE, PE and CE achieve 12.27%, 32.04 l m/W and 27.42 cd/A, respectively.

2. Experimental section

2.1. General methods

All the reagents and solvents for the synthesis were purchased from commercial sources and used directly without further purification. All the reactions were performed in argon atmosphere.^{1}H NMR was recorded with a Varian Gemin-400 spectrometer. Mass spectra were recorded on a PE SCIEX API-MS spectrometer. Elemental analysis (C, H, N) was performed using a Vario EL III CHNS elemental analyzer. UV–vis absorption and photoluminescence (PL) spectrometer were measured on a Perkin-Elmer Lambda 950 UV/vis Spectrometer and a Perkin-Elmer LS50 fluorescence spectrometer, respectively. Absolute PL was measured with a Labsphere™ integrating sphere using a monochromatized Xe lamp (Newport™) as exciting source. Thermogravimetric analysis (TGA) was performed on a TA Instrument TGA-50. The heating rate of TGA was 10 °C min^{-1}. Cyclic voltammetry (CV) was scanned with a CHI600 voltammetric analyzer featuring a three-electrode system (glassy carbon electrode as working electrode, platinum wire as auxiliary electrode, Ag/AgCl as reference electrode). Ferrocene was used as internal standard with an absolute highest occupied molecular orbital level of −4.80 eV. Degassed 0.1 mol/L tetrabutylammoniumhexafluorophosphate CH_2Cl_2 solution was employed as a supporting electrolyte. The HOMO levels were calculated by measuring oxidation potentials. The LUMO energy levels were estimated by subtracting from the HOMO energy levels with optical band gaps. For the theoretical calculation, geometrical properties was optimized at B3LYP/6–31 g(d, p) level using the Gaussian 09 program.

2.2. Device fabrication and measurement

Devices were fabricated on pre-cleaned ITO-coated glass substrates with a sheet resistance of 15 Ω/sq. Before use, the substrates were swabbed with Decon-90 solution, and treated by15 min ultrasonic baths in acetone and deionized water respectively, and then rinsed with isopropanol. The solvent on the surface was removed with by dry N_2 flow, and then the clean substrates were stored in an oven at 120 °C. After a 20 min UV-ozone treatment, the substrates were transferred into a deposition chamber with vacuum better than 10^{-6}Torr. Current density-voltage characteristics and electroluminescence radiation were recorded with a Keithley 2400 power source and a Spectrascan PR650 photometer, respectively. Device measurement was performed under ambient conditions.

2.3. Synthesis methods

2.3.1. 2-(4-(9,9′-spirobi[fluoren]-2-yl)phenyl)-1-phenyl-1H-phenanthro[9,10-d]imidazole (2-PPI—SBF)

A mixture of starting 1 (1.45 g, 2.92 mmol), 2-bromo-9,9′-spirobi[fluorene] (1.15 g, 2.92 mmol), tetratkis(triphenylphosphine)palladium (0) (0.16 g) and 8 ml aqueous K_2CO_3 (8 ml, 2 M) with ethanol (10 ml) and toluene (30 ml) was added into a clean 150 ml flask and reluxed for 24 h under N_2 atmosphere. the organic phase was washed with water and extracted with dichloromethane; then, the extracts were concentrated by rotary evaporation. The residue was further purified by column chromatography (petroleum ether:CH_2Cl_2, 1:4) to get pure white powder (0.95 g, 47.5%).^{1}H NMR (400 MHz, CD_2Cl_2) δ 8.80 (dd, J = 21.8, 8.1 Hz, 2H), 8.07–7.87 (m, 4H), 7.87–7.51 (m, 10H), 7.44 (dd, J = 15.1, 8.6 Hz, 4H), 7.36–7.27 (m, 2H), 7.16 (t, J = 7.5 Hz, 4H), 6.96 (s, 2H), 6.74 (dd, J = 14.4, 7.2 Hz, 3H). MS(ESI$^+$):*m/z* 684.82. Calcd for $C_{52}H_{32}N_2$: (M + H) 685.2633 Anal. Found: C, 91.20; H, 4.71; N, 4.09%. Calcd for $C_{52}H_{32}N_2$: C, 90.08, H, 4.68, N, 3.89%.

2.3.2. 2-(4-(9,9′-spirobi[fluoren]-4-yl)phenyl)-1-phenyl-1H-phenanthro[9,10-d]imidazole (4-PPI—SBF)

The synthetic procedure was similar to that of 2-PPI—SBF. Yield: 51% (1.02 g white powder). ^{1}H NMR (400 MHz, CD_2Cl_2) δ 8.80 (dd, J = 21.8, 8.1 Hz, 2H), 8.07–7.88 (m, 4H), 7.69 (dd, J = 18.6, 8.2 Hz, 8H), 7.55 (d, J = 7.2 Hz, 2H), 7.44 (dd, J = 15.1, 8.6 Hz, 4H), 7.36–7.26 (m, 2H), 7.16 (t, J = 7.5 Hz, 4H), 6.96 (s, 2H), 6.74 (dd, J = 14.4, 7.2 Hz, 3H). MS(ESI$^+$):*m/z* 684.82. Calcd for $C_{52}H_{32}N_2$: (M + H) 685.2632 Anal. Found: C, 91.20; H, 4.71; N, 4.09%. Calcd for $C_{52}H_{32}N_2$: C, 89.82, H, 4.70, N, 3.86%.

3. Result and discussion

3.1. Synthesis and characterization

The synthetic routes of 2-PPI—SBF and 4-PPI—SBF are illustrated in Scheme 1. The starting material 1 were prepared according to the literature [9]. Finally, the classical “Suzuki” reaction [10] was adopted to synthesize the target products 2-PPI—SBF and 4-PPI—SBF with high yields. The compounds were then purified using a silica column and characterized with ^{1}H NMR spectroscopy, mass spectrometry and elemental analysis.

3.2. Thermal properties

The thermal properties of 2-PPI—SBF and 4-PPI—SBF were investigated by thermal gravimetric analysis (TGA) under a nitrogen atmosphere at heating rate of 10 K/min. As shown in Fig. 1, due to the bulky and rigid skeleton of the phenanthroimidazole and spirobifluorene units, the both 2-PPI—SBF and 4-PPI—SBF exhibited high decomposition temperature ($T_{d,}$ corresponding to 5% weight loss) of 400 and 450 °C, respectively. Such good thermal stability is beneficial to the formation of uniform amorphous film upon thermal evaporation, as well as to keep the stability of the film and to decrease the phase separation of the host-guest system when 2-PPI—SBF and 4-PPI—SBF are used as a host material [11]. The detailed data were summarized in Table 1.

3.3. Photophysical properties

The photophysical properties of 2-PPI—SBF and 4-PPI—SBF were investigated by ultraviolet–visible (UV–Vis) absorption and photoluminescence (PL) spectrometry. As shown in Fig. 2, two molecules exhibit similar absorptions in dilute DCM (10^{-5} mol/L), the long

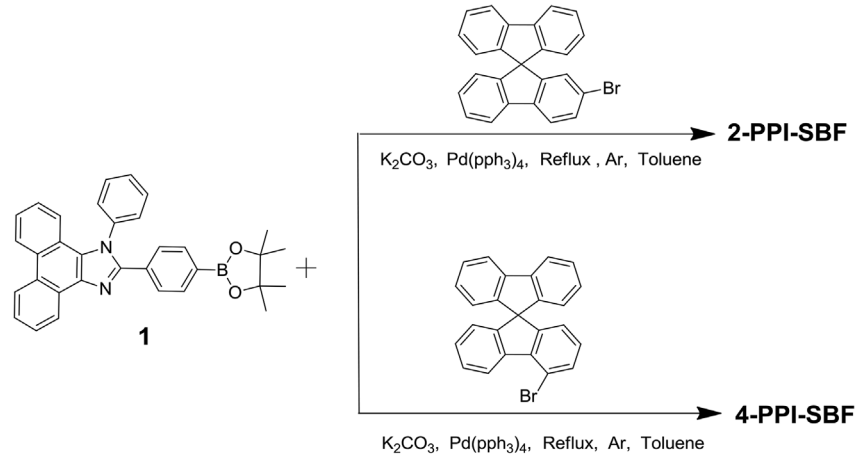

Scheme 1. Synthesis routes of 2-PPI—SBF and 4-PPI—SBF.

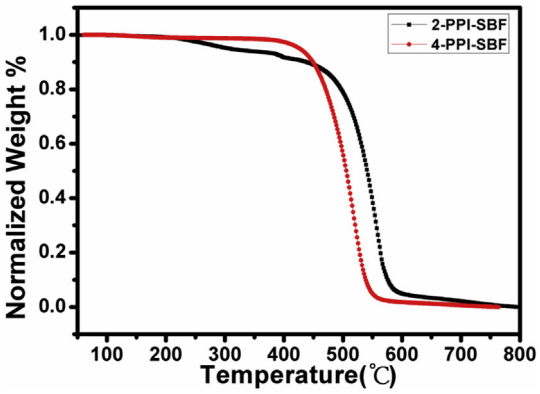

Fig. 1. TGA curves of 2-PPI—SBF and 4-PPI—SBF.

wavelength absorption bands at around 309 nm and 341 nm, which may be attributed to the π-π* transition of the phenanthroimidazole and spirobifluorene group [12]. A strong absorption peak was observed at round 260 nm, which is originated from the π-π* of the benzene ring [13]. the PL properties were studied in dilute DCM (10^{-5} mol/L) and solid state, they exhibit deep-blue emission at 423 nm for 2-PPI—SBF and 428 nm for 4-PPI—SBF in dilute DCM solution with high fluorescence quantum yield (Φ_f = 100% for 2-PPI—SBF, Φ_f = 79.8% for 4-PPI—SBF). Interestingly, two compounds emission peak are located at around 409 nm for 2-PPI—SBF and 413 nm for 4-PPI—SBF with 14 nm blueshifts in the solid film state compared to those in DCM solution. Two materials are predominantly attributed to the formation of a twisted intramolecular charge-transfer (TICT) state in dilute DCM solution, whereas in the solid state, this TICT state is restrained [14]. The absolute Φ_f of 2-PPI—SBF and 4-PPI—SBF was 70.5% and 65.9% by grinding the as-prepared solids into an amorphous state. On the other hand, in order to study the relationship between the molecular structure and luminescent properties, we further investigated different PL spectra of 2-PPI—SBF and 4-PPI—SBF in different polarity solvents. As shown in Fig. S1, with solvents polarity increasing from low-polarity toluene to high-polarity acetonitrile, the emission positions are nearly unchanged (redshifts around at 10 nm), indicating that intramolecular charge transfer (ICT) was effectively controlled. Fig. S2 also shows the phosphorescence spectrum of 2-PPI—SBF and 4-PPI—SBF at the low temperature (77 k). From the spectrum, using the emission peak of phosphorescence, the triplet energy levels of 2-PPI—SBF and 4-PPI—SBF were calculated to be 2.82 eV for and 2.48 eV, respectively. Therefore, two compounds might be promising candidates as both deep-blue emitter and hosts for red and green PhOLEDs and WOLED.

3.4. Theoretical calculation

Electronic molecular orbital calculation result by Gaussian 09 software was analyzed to identify the highest occupied molecular orbital (HOMO) and the lowest unoccupied molecular orbital (LUMO) distribution of 2-PPI—SBF and 4-PPI—SBF. As shown in Fig. 3, the shapes of the HOMO 2-PPI—SBF and 4-PPI—SBF orbitals are similar, mainly located on the phenanthroimidazole moiety, benzene bridges and a small part spirofluorene. The LUMO of 2-PPI—SBF and 4-PPI—SBF are distributed spirofluorene, benzene bridges and small part phenanthroimidazole. It is noted that a part overlapping between the HOMO and LUMO, due to effective electronic communication between the spirobifluorene and phenanthroimidazole unit [15]. On one hand, it would contribute to the balanced charge transfer as the emitter in OLED [16], on the other hand, it facilitates highly efficient luminescence as emitter in OLED, as well as promote the charge transfer process upon excitation [8].

3.5. Electrochemical properties

Cyclic voltammetry (CV) was performed to investigate the

Table 1
The thermal and photophysical properties of 2-PPI—SBF and 4-PPI—SBF.

Compound	T_d/[a] [°C]	λ_{abs} (soln) [nm]	λ_{em}[b] [nm] (soln/film/phos)	Φ_f[c] [%] (soln/film)	HOMO/LUMO[d] [eV]	T_1[e] [eV]
2-PPI—SBF	400	260/309/341	423/409/441	100/70.5	−5.66/-2.38	2.80
4-PPI—SBF	450	260/309/341	428/413/506	77.1/65.9	−5.71/-2.43	2.48

[a] 5% weight loss temperature.
[b] The PL spectra in DCM, neat film and 2-MeTHF glass matrix at 77 K.
[c] The solution-state quantum yield measured in DCM by using 9,10-diphenylanthracene as a standard (Φf = 0.90 in cyclohexane) and the film-state quantum yield on the quatrz plate estimated by an integrating sphere apparatus.
[d] HOMO: calculated from the onset oxidation potentials of the CV cures, LUMO: estimate from the equation: ELUMO = EHOMO + Eg.
[e] Estimated from the phosphorescence spectra at 77 K.

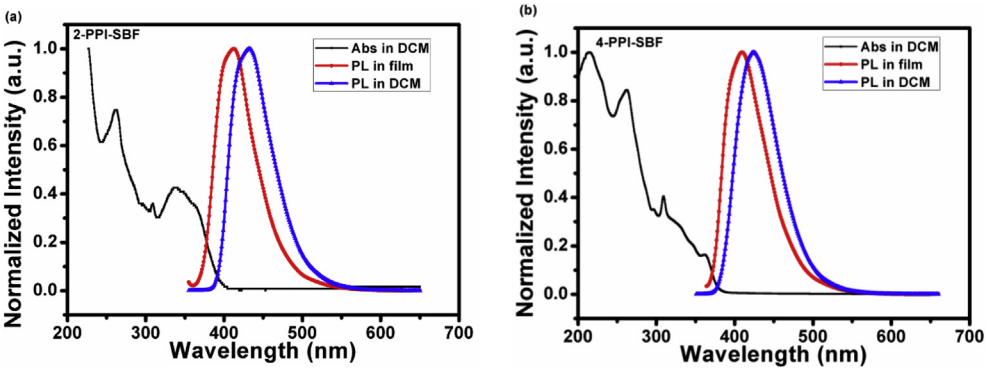

Fig. 2. The UV–Vis absorption and PL spectra in dilute CH_2Cl_2 solution (10^{-5} M) and in the thin film state of 2-PPI—SBF (a) and 4-PPI—SBF (b).

electrochemical properties of 2-PPI—SBF and 4-PPI—SBF. In this experiment, the work and reference electrodes are glass carbon and Hg/$HgCl_2$, respectively. The tetra-*n*-butylammoniumhexa- fluorophosphate (0.1 M in dichloromethane) used as the supporting electrolyte. As shown in Fig. 4, the HOMO levels were measured to be −5.66 for 2-PPI—SBF and −5.71 for 4-PPI—SBF, from the onset of oxidation curves, referring to the equation: HOMO = - (4.80 + E_{ox}) eV [17]. The LUMO of 2-PPI—SBF and 4-PPI—SBF values were obtained by addition of the HOMO value to the band gap (*Eg*) estimated from the onset absorption. The calculated LUMOs are −2.38 and 2.43 eV, respectively.

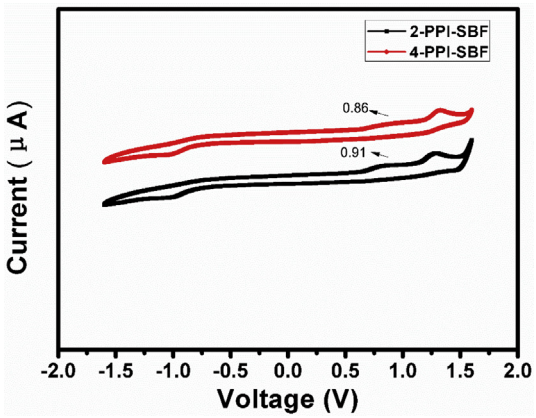

Fig. 4. Cyclic voltammograms (CV) curves of 2-PPI—SBF and 4-PPI—SBF.

3.6. Single-Carrier devices

In order to better understand the effect of the structural change on the energy level and the carrier injection/transport ability, the hole-only and the electron-only devices of 2-PPI—SBF and 4-PPI—SBF were fabricated, respectively. The configuration of the hole-only devices is ITO/NPB(10 nm)/2-PPI—SBF or 4-PPI—SBF (100 nm)/NPB (10 nm)/Al (100 nm) and the electron-only device has the configuration of ITO/TPBI(10 nm)/2-PPI—SBF or 4-PPI—SBF (100 nm)/TPBi(10 nm)/LiF (1 nm)/Al(100 nm). As shown in Fig. 5, it is obvious that both devices can conduct significant current, indicating bipolar transporting ability of both 2-PPI—SBF and 4-PPI—SBF [18]. Additionally, balanced carrier transporting property will be expected to reveal why the devices based on 2-PPI—SBF and 4-PPI—SBF achieved higher current density luminescence at relatively lower turn-on voltage, which is an important factor for the device efficiencies [19].

3.7. Electroluminescent properties

Using the two compounds as emitters, non-doped OLED were fabricated with configuration of ITO/TAPC (40 nm)/TCTA (5 nm)/2-PPI—SBF or 4-PPI—SBF (30 nm)/TPBi (30 nm)/LiF (0.8 nm)Al

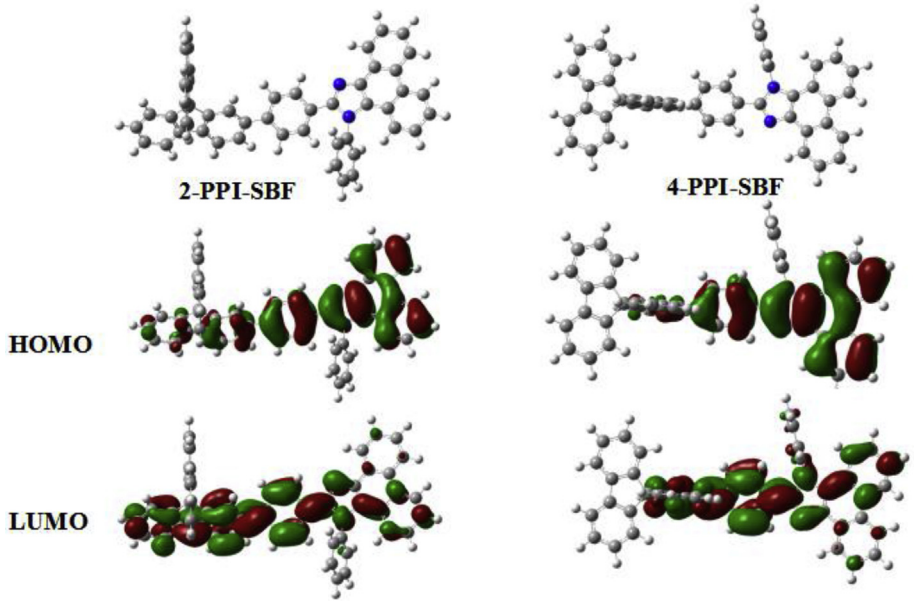

Fig. 3. Optimized structure and spatial distribution of HOMO and LUMO orbitals of 2-PPI—SBF and 4-PPI—SBF.

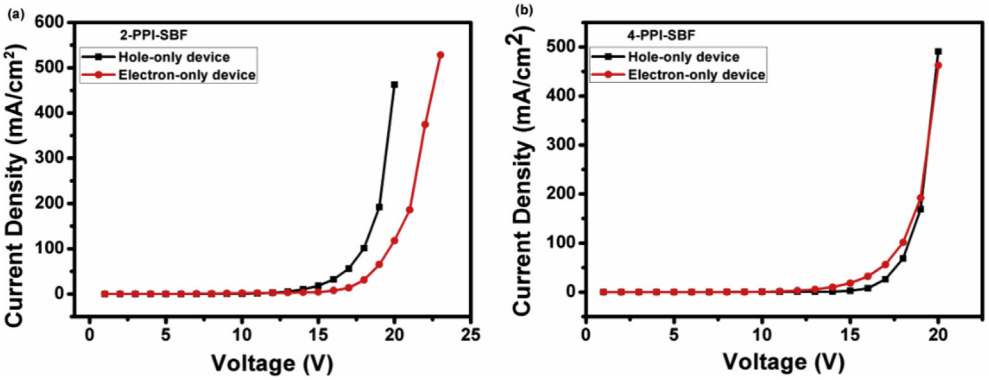

Fig. 5. Current density versus voltage characteristics of the hole-only and electron-only devices for 2-PPI−SBF (a) and 4-PPI−SBF (b).

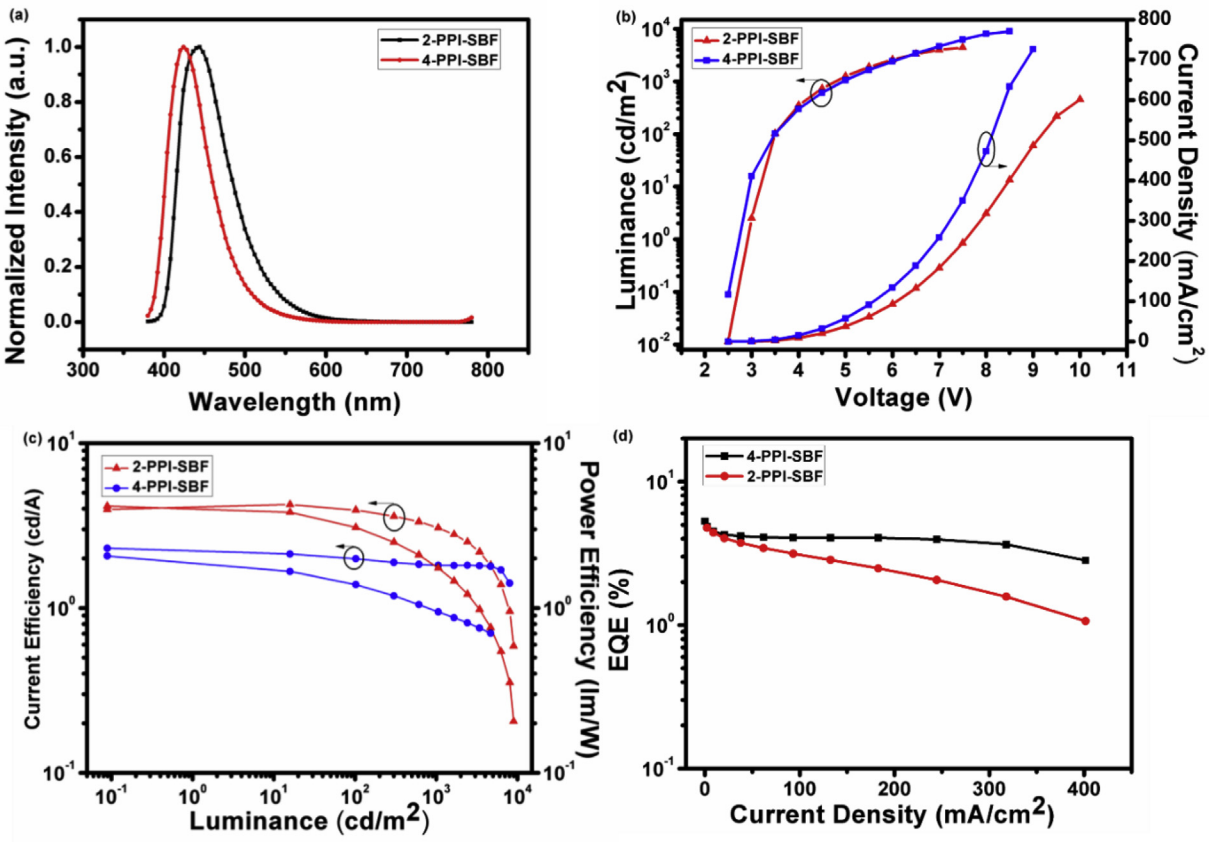

Fig. 6. (a) EL spectra, (b) J-V-L characteristics, (c) Plots of CE and PE versus luminance, (d) EQE of devices based on 2-PPI−SBF and 4-PPI−SBF.

(100 nm). Here, TAPC (1,1-bis[4-[N,N′-d(p-toyl)amino]phenyl]cyclohexane) is hole-transporting layer, TCTA (4,4′,4″-tri(N-carbazolyl)-triphenylamine) is an electron-blocking layer to prevent leakage of excitons into the HTL, TPBi is both the electron-transporting layer and the hole-blocking layer and LiF serve as electron-injecting layer. The EL spectra of devices were shown in Fig. 6a. 2-PPI−SBF and 4-PPI−SBF show a violet-blue emission with peaks at 440 nm and 424 nm, respectively. No new peaks are observed under different operation voltage (Fig. S3), indicating that carrier recombination is well confined within the EML [20]. the devices turn on at very low bias voltages (2.75 eV for 2-PPI−SBF and 4-PPI−SBF), revealing the small carrier injection barrier in the devices [21]. Fig. 6c and d shows the efficiency of the two devices. The 2-PPI−SBF-based non-doped device exhibits the maximum EQE is as high as 4.78%, and corresponding current efficiency (CE) and power efficiency (PE) are 4.24 cd/A and 4.14 l m/W and CIE coordinate of (0.154, 0.105), respectively. 4-PPI−SBF also delivers good EL efficiency, together with an high brightness of 8951 cd/m^2, a maximum EQE, CE and PE of 5.29%, 2.43 cd/A and 2.30 l m/W and CIE coordinate of (0.155, 0.058) respectively. The maximum external quantum efficiency of based on 4-PPI−SBF devices exceed theoretical limit EQE of traditional fluorescence (EQE: 5%). In order to further investigate reasons of device performance high efficiency. We calculated exciton utilization efficiency (EUE) by the Monkman theory [22], which can be represented as following:

$$\mathrm{EQE} = \eta_r \times \eta_{out} \times \Phi_f \times \gamma \quad (1)$$

where η_r is the exciton utilization efficiency, γ is the charge recombination efficiency (assumed as 100% in a properly designed EL device), and η_{out} is the optical out-coupling factor (20% in a device without out-coupling enhancement). For the Φ_f listed in Table 1 (70.5% for 2-PPI−SBF, 65.9% for 4-PPI−SBF), the maximum EUE calculated for 2-PPI−SBF and 4-PPI−SBF are 33.9% and 40.1%. Significantly, the EUE

Table 2
Key performance summary of the 2-PPI−SBF− or 4-PPI−SBF-based blue, green and orange-red emitting devices.

Emitter	V_{on}[a] [V]	λ_{EL} [nm]	CE $_{max}$[b] [cd/A]	PE $_{max}$[c] [lm/W]	EQE $_{max}$[d] [%]	L $_{max}$ [cd/m^2]	CIE [x, y]
B1	2.75	440	4.42	4.14	4.78	4443	(0.154, 0.105)
B2	2.75	424	2.30	2.06	5.29	8951	(0.155, 0.058)
G1	2.8	530	26.03	27.23	6.82	5090	(0.355, 0.601)
G2	2.8	526	64.09	67.92	16.79	69230	(0.333, 0.628)
R1	2.8	605	21.90	22.92	13.07	45630	(0.615, 0.381)
R2	2.8	605	23.88	24.99	14.83	63080	(0.615, 0.384)

[a] V_{on} is the voltage at 1 cd/m^2.
[b] The maximum current efficiency.
[c] The maximum power efficiency.
[d] The maximum external quantum efficiency.

breaks through the theoretical limit of the conventional fluorescent OLEDs (25%) indicating that more excitons are used in 2-PPI−SBF and 4-PPI−SBF due to balanced carrier flux and a broad distribution of recombination regions within the emitting layer. Besides, in devices structure, to use TCTA as buffer layer successfully improve EUE for achieving high efficiency in our work [23]. One the other hand, orbital coupling and electronic communication make triplet excitons reverse to singlet and lead to breakthrough in efficiency [24].

To further investigate the electroluminescence properties, 2-PPI−SBF and 4-PPI−SBF as host materials were studied by fabricating red and green phosphorescent dopants. We fabricated red and green PhOLEDs with the configuration of ITO/MoO_3 (10 nm)/TAPC (40 nm)/EML: (2-PPI−SBF: 10 wt% Ir(MDQ)$_2$(acac) for R1 and 4-PPI−SBF: 10 wt % Ir(MDQ)$_2$(acac) for R2, 2-PPI−SBF: 8 wt% Ir(ppy)$_3$(acac) for G1 and 4-PPI−SBF: 8 wt% Ir(ppy)$_3$(acac) for G2) (30 nm)/TPBi (30 nm)/LiF (0.8 nm)/Al (100 nm), where TAPC and TPBi were used as charge-transporting materials, LiF served as electron-injecting layer, Ir(MDQ)$_2$(acac) doped in host 2-PPI−SBF (R1) and 4-PPI−SBF (R2) was used as the emitting layer. The key data are also listed in Table 2 and the performances are displayed in Fig. 7. EL spectral are shown Fig. 7a, no derivations or new peaks were observed under different operation voltages (Fig. S4), implying that no excitons are wasted for host emission and effective exothermic energy transfer from the host to dopant in the emission layer [25]. The device R2 exhibit a low turn-on voltage of 2.8 V, a high luminance of 63080 cd/m^2. The maximum EQE of 14.83%, CE of 23.88 cd/A and 24.99 l m/W are among the highest values of red phosphorescent OLEDs with blue emitters as hosts. The device R2 shows the maximum luminance of 45630 cd/m^2, the maximum EQE of 13.07%, the maximum PE of 22.92 l m/W and the maximum CE of 21.90 cd/A. In addition, green PhOLEDs with excellent performance were also achieved by employing these two compounds as hosts. As shown Fig. S5, device G2 exhibits the maximum EQE of 16.79%, CE of 64.09 cd/A and PE of 67.92 l m/W. However, device G1 shows a much lower EL efficiency than device G2. The main reason can be attributed to unbalanced carrier transporting properties, resulting in a loss of efficiency. The above electroluminescent experimental results demonstrate that 2-PPI−SBF and 4-PPI−SBF are universal host materials for red and green phosphorescent emitters.

3.8. White light OLED

One of the important applications for deep-blue emitters is the fabrication of white OLEDs (WOLEDs) [26]. the WOLED structure for this study is as follows: ITO/NPB (40 nm)/Ir(btp)$_2$(acac)10 wt%: CBP (10 nm)/Ir(ppy)$_3$ 10 wt%: CBP (4 nm)/CBP (3 nm)/4-PPI−SBF or 2-PPI−SBF (5 nm)/TPBi (40 nm)/LiF (0.8 nm)/Al (80 nm). In the devices, the NBP and TPBi were used as hole transporting layer and electron-transporting layers, respectively. Ir(btp)$_2$(acac)10 wt%: CBP is the red emitting layer, Ir(ppy)$_3$ 10 wt%: CBP is the green emitting layer, 4-PPI−SBF and 2-PPI−SBF are the blue emitting layer. As shown in Fig. 8, three separate peaks, respectively, at 440, 520 and 596 nm for W1 and 420, 524 and 596 nm for W2. The EL spectra show stable and high quality observed. This apparent resistance to the color change under the different voltages well indicates the balanced charge carrier injection and transport for exciton recombination in the three separate emissive regions. As shown Fig. S6, device W2 exhibits intense white light (L_{max} = 61730 cd/m^2) through the simultaneous emission from the primary RGB emitters and shows excellent performance with $\eta_{C,\ max}$, $\eta_{ext,\ max}$ and $\eta_{P,\ max}$ of 32.68 cd/A, 12.27% and 27.78 l m/W, respectively (Fig. S9). The CIE coordinate of (0.367, 0.305) is slightly deviated from the values of the theoretical white point (0.33, 0.33) [27], mainly due to insufficient green and red components in the emission spectrum. The detailed data are listed in Table 3.

4. Conclusions

In summary, we have successfully designed and synthesized two deep-blue emitting materials 2-PPI−SBF and 4-PPI−SBF as hosts for green and red PhOLED. Non-doped devices based on 2-PPI−SBF and 4-PPI−SBF display an high EQE of 4.75% and 5.24% with deep-blue CIE (0.154, 0.105) and (0.155, 0.056), respectively due to their strong deep blue emission and balanced carrier transporting properties. Green device G2 hosted by 4-PPI−SBF achieved $\eta_{c,\ max}$ and $\eta_{p,\ max}$ as high as 64.09 cd/A and 67.92 l m/W, respectively. Red device R2 obtained a low turn-on voltage of 2.8 V, a maximum CE of 23.88 cd/A, a maximum PE of 24.99 l m/W and a maximum EQE of 14.83%. device R1 showed maximum efficiency value of 21.90 cd/A, 22.92 l m/W and 13.07%, respectively. More importantly, an efficient WOLED using 4-PPI−SBF as

Table 3
Key performance of 2-PPI−SBF− and 4-PPI−SBF-based WOLEDs.

Device	V_{on}[a] [V]	L_{max}[b] [cd/m^2]	CE[c] [cd/A]	PE[d] [lm/W]	EQE[e] [%]	CIE
W1	3.75	40610	12.98	8.93	6.79	(0.372, 0.432)
W2	3.50	61730	32.68	27.78	12.27	(0.367, 0.305)

[a] Turn on voltage at 1 cd/m^2.
[b] The maximum luminance.
[c] The maximum current efficiency.
[d] The maximum power efficiency.
[e] The maximum external quantum efficiency.

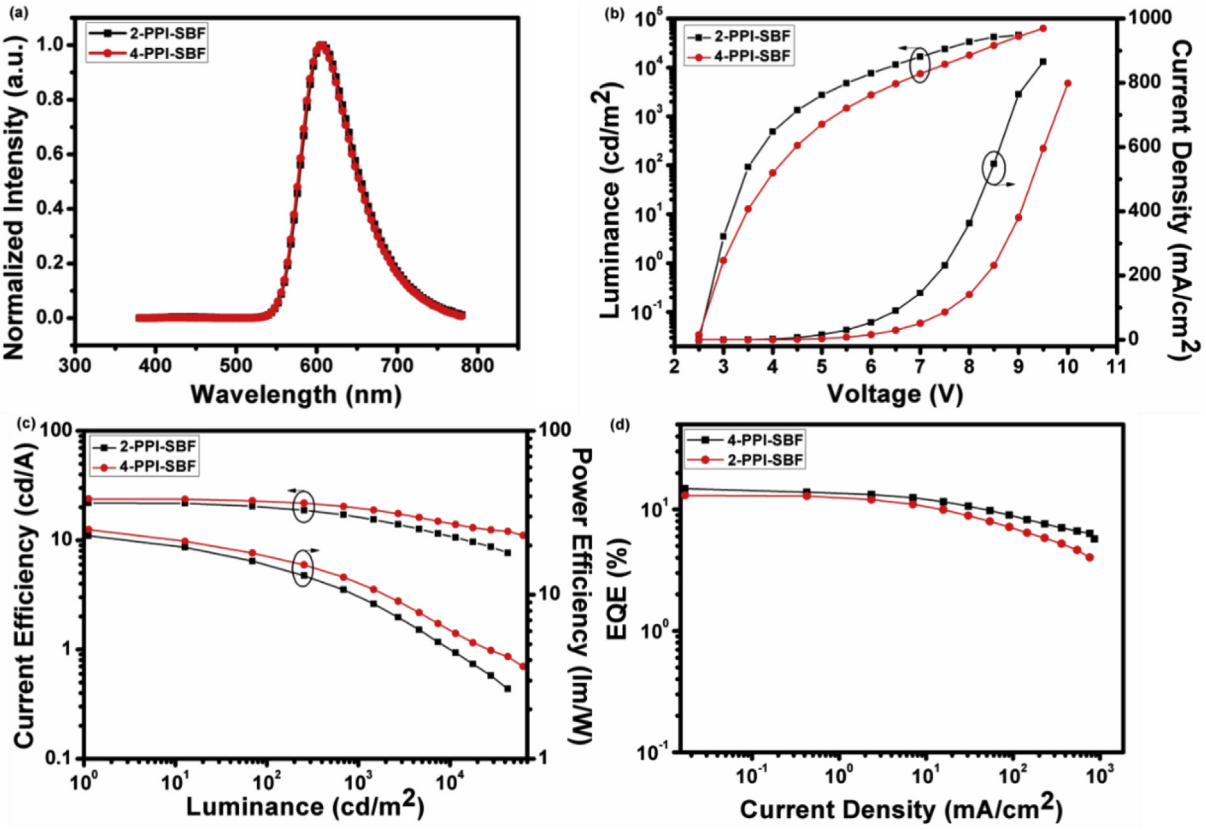

Fig. 7. (a) EL spectra (b) J-V-L characteristics, (c) Plots of CE and PE versus luminance, (d) EQE of devices based on 2-PPI−SBF and 4-PPI−SBF.

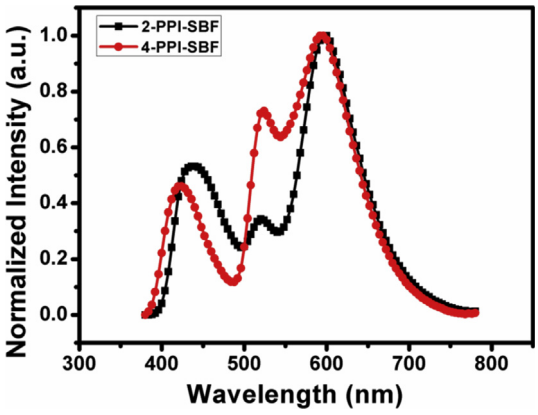

Fig. 8. The EL spectra of multilayer white devices based on 2-PPI−SBF and 4-PPI−SBF.

a deep blue emitter was fabricated and realized pure white light with (0.367, 0.305). All results indicate that the precise molecular design is feasible for developing universal materials for both high performance deep blue emitters and host materials.

Acknowledgments

This research was supported by the National Natural Science Foundation of China (Project No. 51673113). S. L. Tao would like to thank the National Natural Science Foundation of China (NSFC Grant 51373029, 61421002, 51533005), the Preeminent Youth Fund of Sichuan Province (2015JQ0006) and The Fundamental Research Funds for the Central Universities (ZYGX2015J048) for financial support.

Appendix A. Supplementary data

Supplementary data to this article can be found online at https://doi.org/10.1016/j.dyepig.2018.11.058.

References

[1] (a) Tang CW, VanSlyke SA. Appl Phys Lett 1987;51:913;
(b) Song WX, Shi LJ. ACS Appl Mater Interfaces 2018;10:5714;
(c) Chen WC, Yuan Y. Chem Sci 2017;8:3599.
[2] (a) Baldo MA, Thompson ME, Forrest SR. Nature 2000;403:750;
(b) Reineke S, Lindner F, Schwartz G, Seidler N, Walzer K, Lüssem B, Leo K. Nature 2009;459:234;
(c) Grimsdale AC, Chan KL, Martin RE, Jokisz PG, Holmes AB. Chem Rev 2009;109:897;
(d) Choy WCH, Chan WK, Yuan Y. Adv Mater 2014;26:5368.
[3] (a) Kwon J, Park S, Park SY. J Am Chem Soc 2013;135:11239;
(b) Xue S, Yao L, Gu C, Zhang H, Shen F, Xie Z, Wu H, Ma Y. J Mater Chem C 2013;1:7175;
(c) Lin W-C, Huang W-C, Huang M-H, Fan C-C, Lin H-W, Chen L-Y, Liu Y-W, Lin J-S, Chao T-C, Tseng M-R. J Mater Chem C 2013;1:6835;
(d) Dong S, Liu Y, Li Q, Cui L, Chen H, Jiang Z, Liao L. J Mater Chem C 2013;1:6575;
(e) Chen S, Tan G, Wong W-Y, Kwok H-S. Adv Funct Mater 2011;21:3785;
(f) Farinola GM, Ragni R. Chem Soc Rev 2011;40:3467;
(g) Gong SL, Chen YH, Luo JJ, Yang CL, Zhong C, Qin JG, Ma DG. Adv Funct Mater 2011;21:1168;
(h) Yan BP, Cheung CCC, Kui SCF, Xiang HF, Roy VAL, Xu SJ, Che CM. Adv Mater 2007;19:3599;
(i) Sasabe H, Takamatsu JI, Motoyama T, Watanabe S, Wagenblast G, Langer N, Molt O, Fuchs E, Lennartz C, Kido J. Adv Mater 2010;22:5003;
(j) Wang RJ, Liu D, Ren HC, Zhang T, Yin HM, Liu GY, Li JY. Adv Mater 2011;23:2823;
(k) Kamtekar KT, Monkman AP, Bryce MR. Adv Mater 2010;22:572.
[4] (a) Wang K, Wang S, Wei J, Chen S, Liu D, Liu Y, Wang Y. J Mater Chem C 2014;2:6817;
(b) Wang K, Wang S, Wei J, Miao Y, Liu Y, Wang Y. Org Electron 2014;15:3211;
[5] Liu H, Chen P, Hu D, Tang X, Pan Y, Zhang H, Zhang W, Han X, Bai Q, Lu P, Ma YG. Chem Eur J 2014;20:2149.
[6] (a) Huang H, Wang Y, Zhuang S, Yang X, Wang L, Yang CL. J Phys Chem C 2012;116:19458;

(b) Liu B, Zhao J, Luo C, Lu F, Tao SL, Tong QX. J Mater Chem C 2016;4:2003.
[7] (a) Ting HC, Chen YM, You HW, Hung WY, Lin SH, Chaskar A, Chou SH, Chi Y, Liu RH, Wong KT. J Mater Chem C 2012;22:8399;
(b) Jiang W, Tang J, Ban X, Sun Y, Duan L, Qiu Y. Org Lett 2014;16:5346.
[8] Zhang Y, Lai SL, Tong QX, Lo MF, Ng TW, Chan MY, Wen ZC, He J, Jeff KS, Tang XL, Liu WM, Ko CC, Wang PF, Lee CS. Chem Mater 2011;24:61.
[9] Tang X, Bai Q, Peng Q, Gao Y, Li J, Liu Y, Yao L, Lu P, Yang B, Ma YG. Chem Mater 2015;27:7050.
[10] Miyaura N, Suzuki A. Chem Rev 1995;95:2457.
[11] Li WJ, Yao L, Liu HC, Wang ZM, Zhang ST, Xiao R, Zhang H-H, Lu P, Yang B, Ma YG. J Mater Chem C 2014;2:4733. 2.
[12] (a) Chen WC, Yuan Y, Wu GF, Wei HX, Tang Li, Tong QX, Wong FL, S Lee C. Adv. Optical. Mater. 2014;2:626;
(b) Thiery S, Tondelier D, Declairieux C, Geffroy B, Jeannin O, tivier RM, Berthelot JR, Poriel C. J *Phys Chem C* 2015;119:5790.
[13] Li W-J, Liu D, Shen F-Z, Ma D-G, Wang Z-M, Feng T, Xu Y-X, Yang B, Ma Y-G. Adv Funct Mater 2012;22:2797.
[14] Liu B, Yu ZW, He D, Zhu ZL, Zheng J, Yu YD, Xie WF, Tong QX, Lee CS. J Mater Chem C 2017;5:5402.
[15] Yu Y, Wu Z, Li Z, Jiao B, Li L, Ma L, Wang D, Zhou G, Hou X. J Mater Chem C 2013;1:8117.
[16] (a) Li GM, Zhu DX, Peng T, Liu Y, Wang Y, Bryce MR. Adv Funct Mater 2014;24:7420;
(b) Hu DH, Shen FZ, Liu H, Lu P, Lv Y, Liu DD, Ma YG. Chem Commun 2012;48:3015.
[17] Cui LS, Xie YM, Wang YK, Zhong C, Deng YL, Liu XY, Jiang ZQ, Liao LS. Adv Mater 2015;27:4213.
[18] (a) Zhang Y, Ng TW, Lu F, Tong QX, Lai SL, Chan MY, Kwong HL, Lee CS. Dyes Pigments 2013;98:190;
(b) He D, Yuan Y, Liu B, Huang DY, Luo CY, Lu F, Tong QX, Lee CS. Dyes Pigments 2017;136:347;
(c) Pu YJ, Nakata G, Satoh F, Sasabe H, Yokoyama D, Kido J. Adv Mater 2012;24:1765.
[19] (a) Chopra N, Lee J, Zheng Y, Eom SH, Xue J, So F. ACS *Appl Mater Interfaces* 2009;1:1169;
(b) Zhu ZL, Ni SF, Chen WC, Yuan Y, Tong QX, Wong FL, Lu F, Lee CS. Dyes Pigments 2017;146:219;
(c) Tang X, Yao L, Liu H, Shen F, Zhang S, Zhang H, Lu P, Ma Y. Chem Eur J 2014;20:2149.
[20] Zou J, Wu H, Lam CS, Wang C, Zhu J, Zhong C, Hu S, Ho CL, Zhou GJ, Wu H, Choy WH, Peng J, Cao Y, Wong WY. Adv Mater 2011;26:2976.
[21] Yao L, Zhang S, Wang R, Li W, Shen F, Yang B, Ma YG. Angew Chem 2014;126:2151.
[22] Chiang C-J, Kimyonok A, Etherington M-K, Griffiths G-C, Jankus V, Turksoy F, Monkman A-P. Adv Funct Mater 2013;23:739.
[23] (a) Yuan Y, Chen J-X, Lu F, Tong Q-X, Yang Q-D, Mo H-W, Ng T-W, Wong F-L, Guo Z-Q, Ye J, Chen Z, Zhang X-H, Lee C-S. Chem Mater 2013;25:4957;
(b) Cao Y, Parker I-D, Yu G, Zhang C, Heeger A-J. Nature 1999;397:414;
(c) Yao L, Zhang S-T, Wang R, Li W-J, Shen F-Z, Yang B, Ma Y-G. Angew Chem 2014;126:2151;
(d) Lv X-L, Zhang W-Z, Ding D-X, Han C-M, Huang Z, Xiang S-P, Zhang Q, Xu H, Wang L. Adv. Opt. Mater. 2018;6:1800165.
[24] (a) Cao Y, Parker I-D, Yu G, Zhang C, Heeger A-J. Nature 1999;397:414;
(b) Yao L, Zhang S-T, Wang R, Li W-J, Shen F-Z, Yang B, Ma Y-G. Angew Chem 2014;126:2151;
(c) Duan C-B, Han C-M, Du R-M, Wei Y, Xu H. Adv. Optical Mater. 2018;6:1800437.
[25] (a) Wang H, Meng L, Shen X, Wei X, Zheng X, Li X, Yi Y, Wang Y, Wang PF. Adv Mater 2015;27:4041;
(b) Liang Q-Q, Han C-M, Duan C-B, Xu H. Adv. Opt. Mater. 2018;6:1800020.
[26] (a) Lee BM, Kim NH, Yoon JA, Lee SE, Kim YK, Kim WY, Mascher P. J Lumin 2014;148:72;
(b) Ying L, Ho CL, Wu HB, Cao Y, Wong WY. Adv Mater 2014;26:2459.
[27] Qin W, Yang ZY, Jiang Y, Lam JWY, Liang GD, Kwok HS, Tang BZ. Chem Mater 2015;27:3892.